[AMERICAN JOURNAL OF SCIENCE, VOL. 297, JUNE, 1997, P. 651–678]

GRANITE INTRUSION ALONG STRIKE-SLIP ZONES IN EXPERIMENT AND NATURE

TERESA ROMÁN-BERDIEL,* DENIS GAPAIS, and JEAN-PIERRE BRUN

Géosciences Rennes, CNRS, Université de Rennes 1, 35042 Rennes Cedex, France

ABSTRACT. Granite intrusion in the upper crust along a crustal-scale shear zone has been modelled by injecting a Newtonian fluid (low-viscosity silicone putty) into a sandpack containing a ductile layer of silicone putty which acted as a weak level along which the injected material could spread. The strike-slip regime was obtained using two mobile rigid basal plates sliding horizontally. Boundary conditions were chosen in order to analyse the influence of thicknesses of the brittle cover and of the volume of injected material on the pattern of the intrusion. Experiments showed that (1) the presence of a soft layer between two competent units allowed the formation of laccolithic intrusions by lateral expansion in the emplacement site, (2) intrusions are elongate and their long axis tends to track the principal stretching direction associated with the strike-slip regime, (3) this direction controls the emplacement beginning with the first stages of injection, (4) the lateral expansion of the intrusion is locally controlled by arrays of Riedel faults formed in the overburden, (5) the control of faults on the intrusion pattern increases with increasing brittle/ductile ratio, i.e. with increasing depth and (or) decreasing thickness of the weak layer, (6) intrusions are sigmoidal or lozenge shaped in horizontal view, (7) the greater the brittle/ductile ratio, the less sigmoidal are the intrusions, (8) feeding pipes shifted with respect to the strike-slip zone result in asymmetric intrusions, with the development of a sheared tail trailing behind the intrusion.

Examples of leucogranites of the South Armorican Shear Zone (South Brittany, France) emphasize that our experiments can explain the geometry of many syntectonic granites emplaced along strike-slip zones. They further shed some light on mechanisms of pluton intrusion in the upper crust.

INTRODUCTION

Structural controls on granite emplacement have been extensively discussed and documented in the literature (see reviews by Castro, 1987; Hutton, 1988; Pitcher, 1992). Relationships of some plutons to crustal-scale shear zones are particularly well documented. Examples include the Donegal batholith in Ireland (Pitcher and Berger, 1972; Hutton, 1982), the Saraya batholith in Eastern Senegal (Pons, Oudin, and Valero, 1992), the Coastal batholith in Peru (Pitcher and Bussell, 1977), or the Carboniferous granites of the Variscan Chain of western Europe (Berthé, Choukroune, and Jégouzo, 1979; Iglesias and Choukroune, 1980; Jégouzo, 1980; Vigneresse and Brun, 1983; Lagarde, Ait-Omar, and Roddaz, 1990; Aranguren and Tubia, 1992).

* Dpto Geología, Facultad de Ciencias, Universidad de Zaragoza, 50009 Zaragoza, Spain

A question extensively debated about granitic intrusions is the space needed for their emplacement (Hutton and others, 1990; Tikoff and Teyssier, 1992; Paterson and Fowler, 1993a), especially in strike-slip regimes, where the bulk principal compressive stress is horizontal. Models include forcible emplacement within ductile country rocks, as in models of ballooning (Ramsay, 1989) or of in situ lateral expansion (Brun and others, 1990; Lagarde, Brun, and Gapais, 1990) (fig. 1A and B), and various models where space is created at sites of local extension (fig. 1C-H). Thus, several granites associated with major wrench zones have been interpreted as emplaced in zones of local dilatancy (Davies, 1982), in extensional segments of shear zone arrays, like Riedel faults or releasing bends (Mc Caffrey, 1992) (fig. 1C), in the extensional tip areas of shear zones (White and Hutton, 1985; Hutton, 1988; Lagarde, Ait-Omar, and Roddaz, 1990) (fig. 1D), in contractional tip areas of shear zones where along-strike displacements can provide a potential hole for pluton emplacement by bending of country rocks (Hutton, 1981) (fig. 1E), in extensional bridges (D'Lemos, Brown, and Strachan, 1992; Tikoff and Teyssier, 1992) (fig. 1F) or pull-apart fault systems (Guineberteau, Bouchez, and Vigneresse, 1987; Schmidt, Smedes, and O'Neill, 1990), (fig. 1G), or in tension gashes (Castro, 1986; Hutton, 1988) (fig. 1H). This latter process may be efficient in providing channels for magma ascent, rather than able to provide emplacement sites for crustal-scale intrusions. Nevertheless, Hutton (1988) has suggested that injection along dilational fractures can build up large intrusive bodies by successive emplacement of coalescing sheeted dikes, following a process roughly comparable to a crack-seal mechanism.

In all types of models mentioned above, stopping and assimilation may accompany the emplacement of intrusions.

Hutton (1988) emphasized that emplacement processes can actually differ significantly from one pluton to another because of the large range of possible combinations between external tectonic forces and internal buoyancy forces. The various models listed above, which involve various combinations of faulting and continuous deformation, emphasize that the mechanical behavior of the country-rocks, and hence the rheological layering of the crust, are also critical factors controlling the emplacement mechanism.

Many plutons are emplaced at rather shallow crustal levels and probably reached their emplacement site by rising up through a brittle basement along fractures or dikes (Castro, 1986; Clemens and Mawer, 1992) before stopping and spreading within overlying softer sedimentary cover-rocks (Brun and others, 1990; Lagarde, Brun, and Gapais, 1990). In this paper, we present physical models of intrusion in the upper crust along crustal-scale strike-slip zones. Results are compared with examples of syntectonic granites emplaced along the South Armorican Shear Zone (South Brittany, France). They shed some light on first-order interactions between strike-slip tectonics and mechanisms of granite emplacement.

EXPERIMENTAL PROCEDURE

Previous works.–Since pioneer works of Cloos (1928) and Riedel (1929), many experimental studies have been dedicated to strike-slip faults (Oertel, 1965;

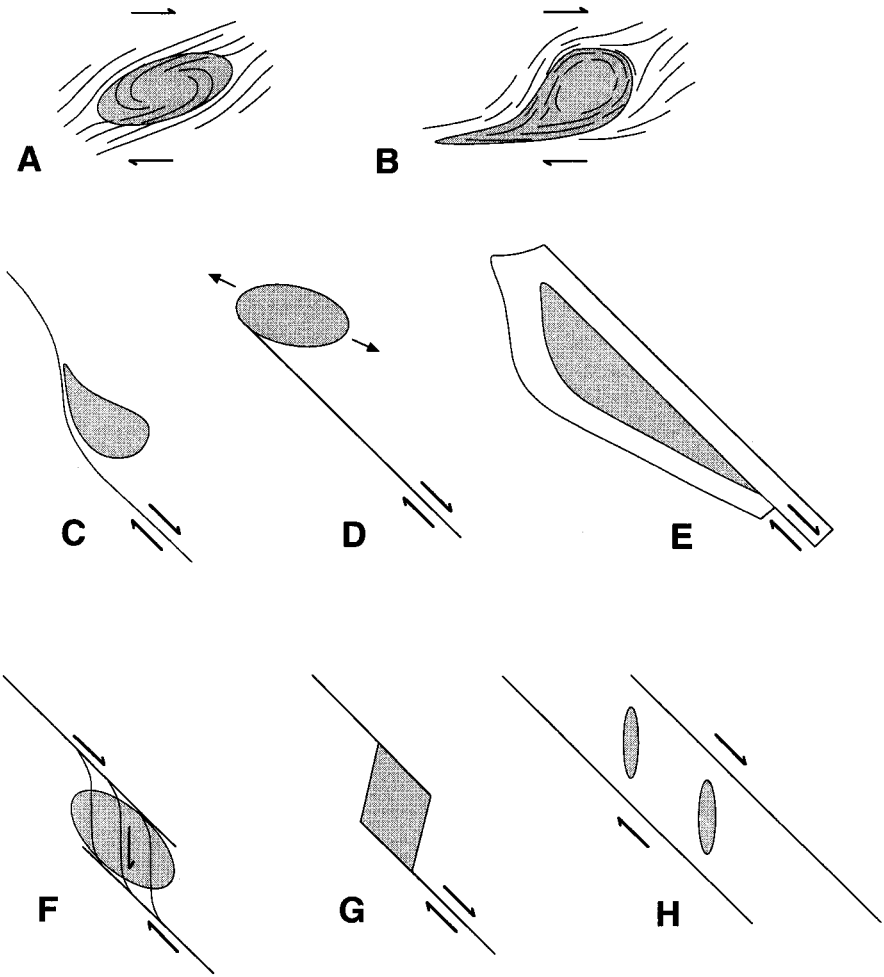

Fig. 1. Diagrammatic map views showing general relationships between upper-crustal syntectonic granite intrusions and strike-slip faults or shear zones according to main emplacement mechanisms proposed in the literature. (A and B) show forcible symmetric and asymmetric intrusions in a ductile environment, and associated cleavage trajectories. (C to H) show various models of emplacement within local extensional contexts. See text for references and further explanations.

Hoppener, Kalthoff, and Schrader, 1969; Tchalenko, 1970; Wilcox, Harding, and Seely, 1973; Emmons, 1979; Naylor, Mandl, and Sijpesteijn, 1986; Richard and others, 1989; Basile, 1990; Richard, Mocquet, and Cobbold, 1991; Gapais, Fiquet, and Cobbold, 1991). Several studies have used sand and silicone putty as analogues of brittle and ductile layers of the crust,

respectively (Richard and others, 1989; Basile, 1990; Richard, Mocquet, and Cobbold, 1991). These studies demonstrated that the deformation associated with strike-slip zones of crustal scale can be conveniently modelled in the natural gravity field using properly scaled sand-silicone models.

On the other hand, many models of gravity-induced diapiric intrusions have been made using ductile materials such as clay, oil, or silicone putty for both buoyant and sinking layers (Grout, 1945; Ramberg, 1970 and 1981; Berner, Ramberg, and Stephansson, 1972; Dixon, 1975; Cruden, 1990). These models, where both intrusion and country-rocks are ductile, applied to deep processes which may occur in the crust below the brittle-ductile transition. On the other hand, when a fluid magma reaches high and possibly brittle crustal levels strength contrasts between intrusion and country-rocks are large. Several experimental studies of laccolithic intrusions have used rather stiff materials to model the country rocks (Howe, 1901; McCarthy, 1925; Hurlbut and Griggs, 1939; Pollard and Johnson, 1973; Dixon and Simpson, 1987). Only a few recent experiments have considered cases where faulting of country-rocks could accompany intrusion (Merle and Vendeville, 1992; Román-Berdiel, Gapais, and Brun, 1995). Román-Berdiel, Gapais, and Brun (1995) have shown that properly scaled sand-silicone putty models can be used to study intrusion processes in the upper crust. In particular, they have shown that the occurrence of a ductile weak layer interbedded within the brittle crust was the first-order factor controlling the formation of a conformable laccolith versus a piercing diapir. Several previous experiments showed that weak layers, such as shales, pelites, or salt, within the brittle crust were conveniently modelled using silicone layers (Ballard and others, 1987; Vendeville, 1987; Richard, Loyo, and Cobbold, 1989; Basile, 1990; Richard, Mocquet, and Cobbold, 1991).

Models described by Román-Berdiel, Gapais, and Brun (1995) were either intrusions in a static environment, or intrusions during extensional deformation. In this paper, we concentrate on analogue models of magma intrusion during regional strike-slip deformation. To our knowledge, this type of experiment has never been described.

Experimental setting and materials.–In most of our experiments, the strike-slip motion was imposed at the base of the model by two thin mobile rigid plates 1 × 0.5 m, lying on a fixed plate, and separated from each other by 3 cm (fig. 2A). Mobile plates were moved in opposite directions at constant rate by screw jacks driven by a stepper motor. This configuration with two basal discontinuities induces a relatively wide strike-slip shear zone in the models (>5 cm). It thus allowed intrusions within the zone, above a fixed injection tube (10 mm diam) located between the two mobile plates (fig. 2A). During strike-slip motion, the fluid was pushed in the tube by a piston driven at constant velocity by a stepper motor (fig. 2B). To ensure a distributed shearing between the mobile plates at the base of the models, a band of silicone putty (80 cm × 6 cm × 1 cm) was placed on the basal velocity discontinuities (fig. 2A and B) (Basile, 1990). The models were centered on the injection point. They are 80 cm in length, 30 cm in width, and have a

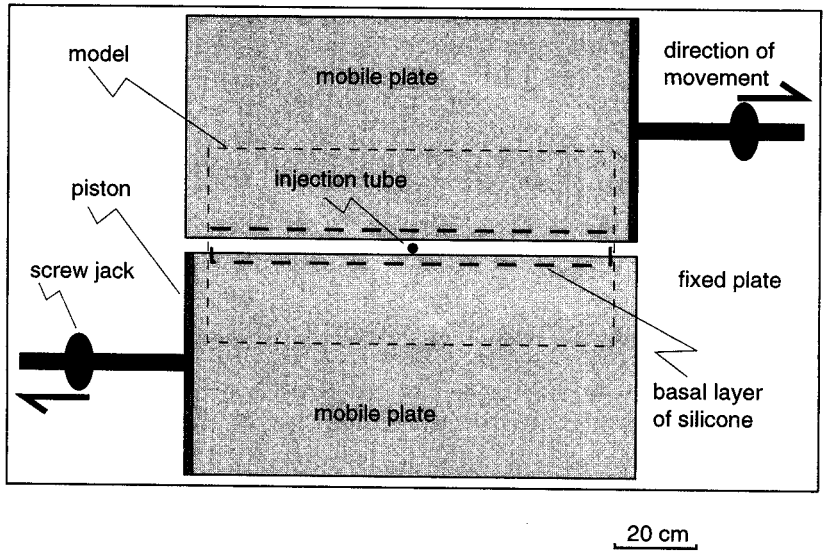

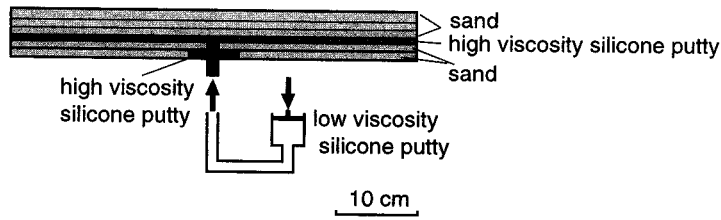

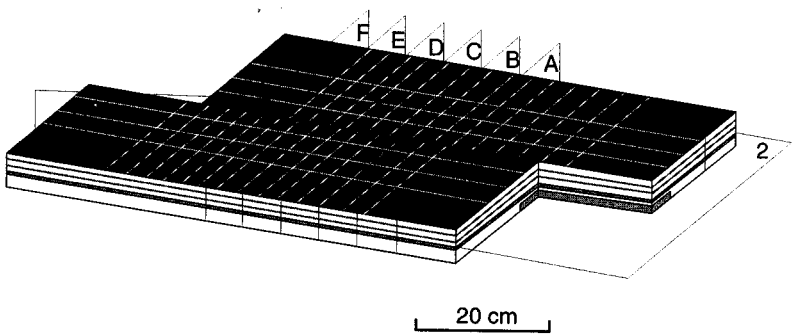

Fig. 2. Sketch of experimental setting. (A) horizontal-view, (B) vertical view, (C) different types of sections used to describe models; vertical sections (1) and horizontal sections (2) are reconstructed from serial vertical sections (A-F) made in models after deformation.

variable height. Lateral boundaries are free, and the models are sufficiently large to prevent significant boundary effects in their central part. In a second set of experiments, the injection was made beside the basal shear zone. In these experiments, we used a single mobile basal plate.

For the brittle crust, we used dry Fontainebleau sand, which is almost pure quartz, with a maximum grain size of 500 μm. Its density depends on its degree of compaction (1300-1800 Kg m^{-3}) (Krantz, 1991). For the layer thicknesses used in our experiments, the mean density is approx 1500 Kg m^{-3}. Dry Fontainebleau sand has an internal friction angle of about 30° and a negligible cohesion (Mandl, De Jong, and Maltha, 1977). For ductile materials, we used silicone putty (GS1R gum of Rhône-Poulenc), which is almost perfectly Newtonian (Vendeville and others, 1987). Two different types of silicone have been used (table 1). A standard, high viscosity silicone was used to introduce soft ductile layers within the sandpack. A low-viscosity silicone was used for the intrusion. The room temperature was 30°C in all experiments.

TABLE 1

Physical properties of model materials. μ is viscosity, and ρ is density

	μ (Pa.s)	ρ (Kg/m^3)
high viscosity silicone	$7,5 \times 10^3$	1270
low viscosity silicone	$2,5 \times 10^3$	1330
dry quartz sand	–	1500

Scaling and boundary conditions.–Models have been scaled following principles discussed by Hubbert (1937) and Ramberg (1981). The scaling used here is similar to that used and described in detail by Román-Berdiel, Gapais, and Brun (1995). We used a length ratio of 10^5, so that 1 cm in models is equivalent to 1 km in nature. Given the ratio of density of natural rocks relative to the analogue materials (of the order of 1), the length ratio used yields a stress ratio of the order of 10^5 of nature relative to model. In others words, the models are about 10^5 times weaker than the natural crust. The time ratio is 10^9 (1 h represents 115000 yrs). According to the experimental scaling of Román-Berdiel, Gapais, and Brun (1995), magma driving pressures of the order of 50 MPa, comparable to those inferred for natural situations (Johnson and Pollard, 1973), are properly scaled relative to both length and time using linear injection rates of the order of 30 cm/h. We used a linear injection rate of 31.2 cm/h (table 2), which scales to 10^{-8} m s^{-1} (27 cm/year) in nature.

For slow displacement rates and consequently slow strain rates, the silicone putty offers a negligible resistance and behaves like a fluid. For the range of velocities used in our models (table 2), scaling for viscosities is therefore not critical.

Modelling of syntectonic intrusion requires a convenient balance between injection dynamics and large-scale boundary conditions. Rather rapid cooling rates are expected for a magma emplaced at high crustal levels, that

TABLE 2

Model characteristics and experimental conditions for the different experiments performed. Models I-2 and II-2 are the same. "Displacement rate" refers to the rate of displacement of each basal plate relative to the intrusion pipe

Series	Model	Thickness of sand layer below injection point(cm)	Thickness of weak layer (cm)	Thickness of sand overburden (cm)	Volume of injected silicone (cm^3)	Brittle/ductile Ratio	Displacement rate (cm/h)	Injection Velocity (cm/h)	Total displacement at model surface (cm)
Single layer	1	1	-	2.0	49	3.00	10	31.2	20.4
Three layer-I	1	1	0.6	1.0	49	1.25	10	31.2	20.0
	2	1	0.6	2.0	49	1.87	10	31.2	20.0
	3	1	0.6	3.0	49	2.50	10	31.2	19.2
	4	1	0.6	4.0	49	3.12	10	31.2	19.4
Three layer-II	1	1	0.6	2.0	98	1.87	5	31.2	19.8
	2	1	0.6	2.0	49	1.87	10	31.2	20.0
	3	1	0.6	2.0	12	1.87	10	31.2	9.6
Three layer-III	1	1	0.3	1.5	49	1.90	10	31.2	19.2
Three layer-IV	1	1	0.6	2.0	49	1.87	10	31.2	9.6
	2	1	0.6/-	2.0/2.6	49	1.87/3.60	10	31.2	10.0

is, in a low-temperature environment (Spera, 1980). Once substantially cooled, the intrusion and the hornfelsed country-rocks can tend to resist subsequent deformation. This behavior is not represented in our experiments. Consequently, the bulk strike-slip motion was only applied during injection to avoid post-emplacement deformation. Our experimental study of interactions between pluton emplacement and tectonics requires that (1) the overall syn-intrusion deformation is sufficiently large, and (2) injection rates are sufficiently slow to ensure proper scaling. For these reasons and also because stepper motors did not allow for very slow displacement rates ratios between injection rate and bulk strike-slip motion are relatively small (table 2) compared with what might be expected in many natural situations (Paterson and Tobisch, 1992). Nevertheless, because strain accelerations are negligible in models and strain rates used are slow, scaling for time is not a critical factor for these experiments.

Types of model layering.–Two types of analogue models have been made using the first experimental configuration defined by two basal velocity discontinuities and a feeding pipe located in the middle of the strike-slip zone (fig. 2A) (table 2).

The first type of model consisted of single-layer sand packs. Our purpose was to observe the geometry of magma intrusion in a homogeneous brittle crust undergoing strike-slip deformation. The injection was made 1 cm above the base of the sand pack.

The second type of models consisted of three layers made of a sand pack containing an interbedded layer of high-viscosity silicone putty. The injection was made at the base of the soft level. These models can compare to natural situations where a magma reaches a sedimentary cover containing soft layers, like shales, after having rised along faults throughout an underlying resistant basement.

In static models that were otherwise similar to ours, Román-Berdiel, Gapais, and Brun (1995) have shown that the formation of laccolithic intrusions required the presence of a weak ductile layer interbedded within more resistant crustal materials. These authors have thus observed either piercing intrusions which break the surface or conformable laccolithic intrusions localized within the weak layer, depending on the ratio between the thickness of the weak layer and the thickness of the sand overburden (fig. 3). The range of layer thicknesses chosen in most experiments of the present work corresponds to intermediate situations, where unconformable intrusions (that is, partially piercing) of laccolithic shapes are expected to occur (fig. 3) (Three layer models I-2, I-3, II, and IV, table 2). This choice ensured (1) that interactions between intrusions and faulting in the overburden would be possible, and (2) that possible effects of faulting due to strike-slip motion would not be totally overprinted by deformations induced by complete piercement of the overburden.

In all models, the sandpack contained horizontal passive markers made of colored sand, and the silicone layer contained vertical passive markers. At the end of each experiment, these markers allowed us to observe the deformation on cross sections. A grid of square passive sand markers drawn

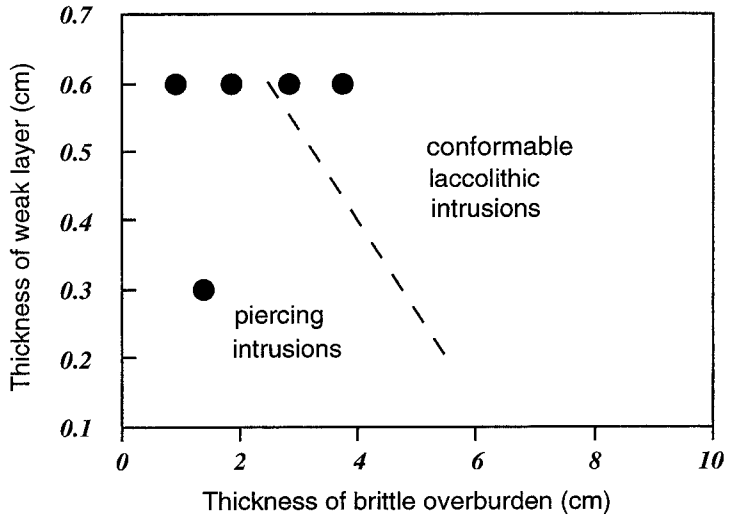

Fig. 3. Experimental fields of piercing intrusions and of conformable laccoliths (separated by a dashed line) according to relative thicknesses of weak silicone layer and sand overburden, as observed in the three layer models of Román-Berdiel, Gapais, and Brun (1995). Black dots show experimental conditions for three layer models described in the present paper. See text for further explanations.

on the upper surface of the models allowed for examination of surface deformation during experiments (see fig. 4).

The 3-D geometry of intrusive bodies was studied on series of cross sections cut perpendicular to the bulk shearing direction at the end of each experiment (fig. 2C). Cross sections parallel to the maximum elongation of intrusions and horizontal maps at depth were reconstructed from serial cross sections (fig. 2C).

Types of experiments performed.–Two main series of three-layer experiments were made (table 2). Both were made at constant thickness of the weak layer (6 mm). In the first series (Three-layer-I, table 2), the volume of injected silicone was kept constant, and the thickness of the overburden was different in each experiment. The second series of experiments (Three-layer-II, table 2) corresponds to injections of different volumes of silicone within the same crustal layering. An additional experiment was made (Three layer-III, table 2) in order to examine the effects of a thinner weak layer (3 mm).

For the second set of experiments characterized by a single basal velocity discontinuity, we made two models where the injection was made beside the velocity discontinuity, thus leading to intrusions shifted with respect to the middle of the strike-slip zone. Models were also made of three layers. In one experiment (Three layer IV-1, table 2), a weak layer was present on both sides of the shear zone; whereas it was only present above the mobile plate in the other experiment (Three layer IV-2, table 2). The purpose of these experiments was to produce asymmetric intrusions.

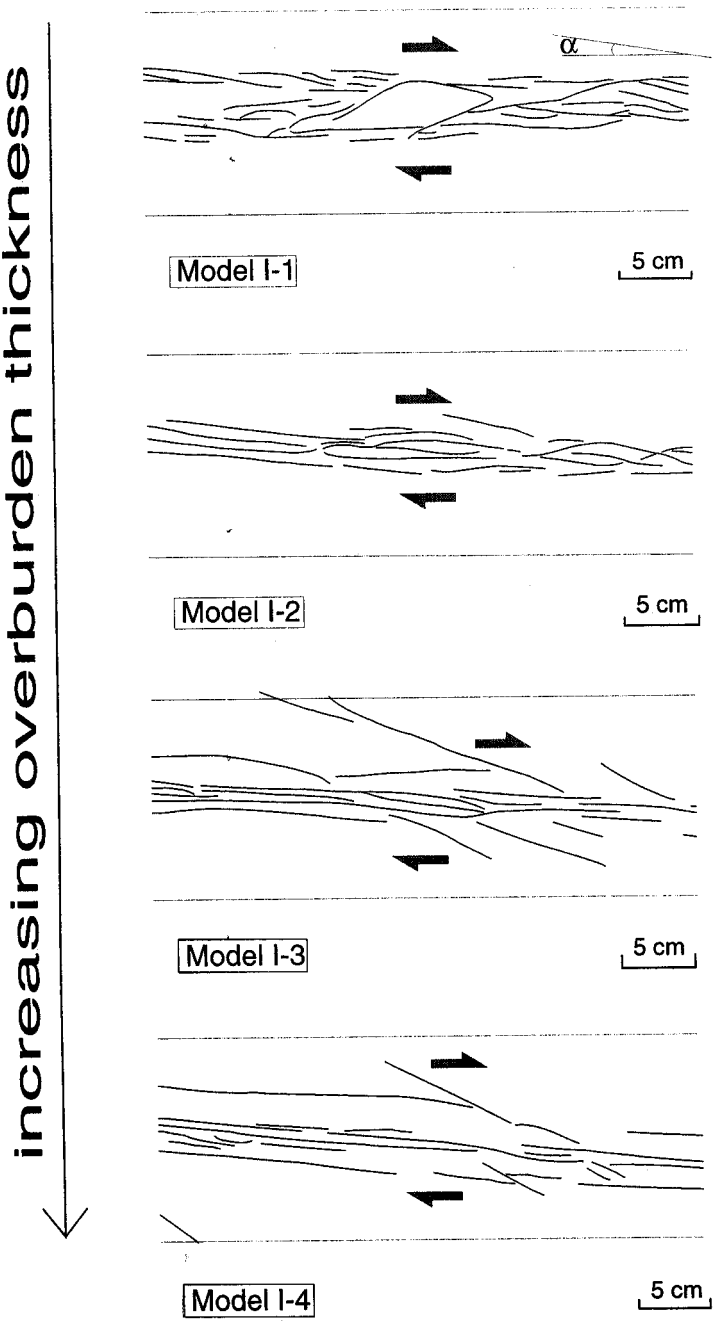

Fig. 4. Line drawings and photographs of surface of representative three layer models with same weak layer thickness and different overburden thicknesses: (A) model I-1, (B) model I-2, (C) model I-3, (D) model I-4. α, angle between synthetic faults and bulk shearing direction (see table 3).

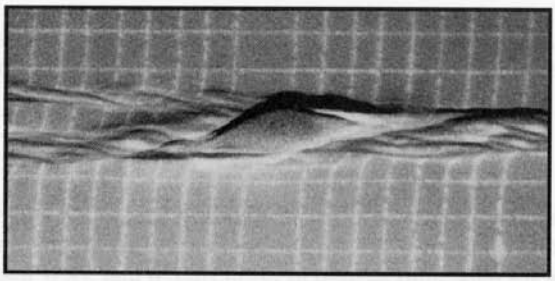

A

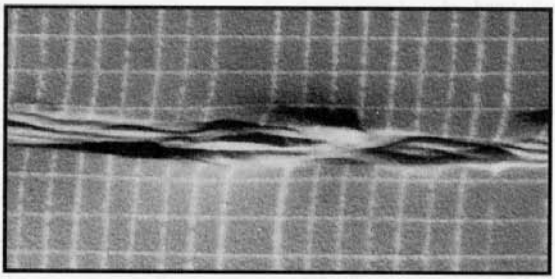

B

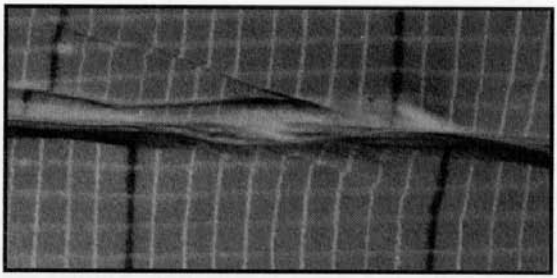

C

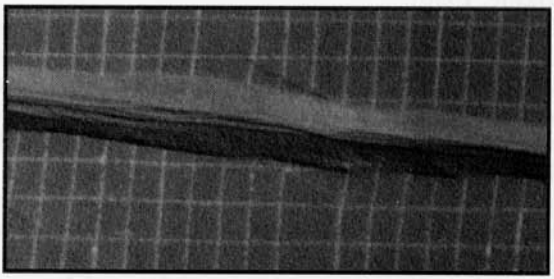

D

Fig. 4 (Continued)

EXPERIMENTAL RESULTS

Fault patterns.–In all experiments, the fault pattern developed in the sand overburden consisted of synthetic faults showing two main sets of orientation (fig. 4; table 3).

TABLE 3

Horizontal trends of major features of model intrusions and faults with respect to bulk shearing direction (angles are counted positive in counterclockwise sense). θ′ and ρ were measured on the horizontal sections at depth (figs. 8 and 9); α was measured at the surface of the models (fig. 4); γ, bulk shear strain for each model.

Model	Overall trend of intrusion elongation (θ′)°	Local trends of second-order intrusion boundaries (ϕ)°	Overall orientation of main sets of synthetic faults (α)°		Bulk shear strain (γ)
Single layer-1	7	-11,-29	-6	-24	6.8
Three layer-I-1	11	0	0,-4	---	6.7
Three layer-I-2	9	0,-15	-6	---	6.7
Three layer-I-3	10	-16,-21	-4	-20	6.4
Three layer-I-4	2	-6,-26	-6	-26	6.5
Three layer-II-1	10	-10,-26	-4	-10,-22	6.6
Three layer-II-3	15	-8,-19	-2	-13	3.2
Three layer-III-1	11	-11,-14	-7	-12	6.4
Three layer-IV-1	10		0	-16	3.2
Three layer-IV-2	12		-12		3.3

Numerous faults at low angle to the bulk shearing direction (Y and P faults) occur within the main deformation zone. Oblique faults with Riedel attitude are less numerous and occur mainly in the less deformed areas on both sides of the main deformation zone (models I-3 and I-4, fig. 4C and D). This pattern results from early development of Riedel faults which are subsequently overprinted by faults at low angle to the bulk shearing direction during progressive strike-slip and strain localization. Similar scenarios are classical in strike-slip experiments (Tchalenko, 1970; Naylor, Mandle, and Sijpesteijn, 1986; Basile, 1990).

At constant thickness of the weak layer, discrete oblique Riedel faults are well developed in experiments with relatively thick sand overburden (models I-3 and I-4, fig. 4C and D); whereas more distributed arrays of faults at low angle to the bulk shearing direction are observed in experiments with thinner overburden (models I-1 and I-2, fig. 4A and B) (table 3). Such reductions in degree of strain localization and in angle between major faults and bulk shearing direction with decreasing overburden have been attributed to an increase of the mechanical coupling between sand and silicone layers with decreasing brittle/ductile ratio (Basile, 1990).

Effect of the weak layer.–Injection within a single sand layer resulted in massive intrusions cutting along steep boundaries throughout the entire

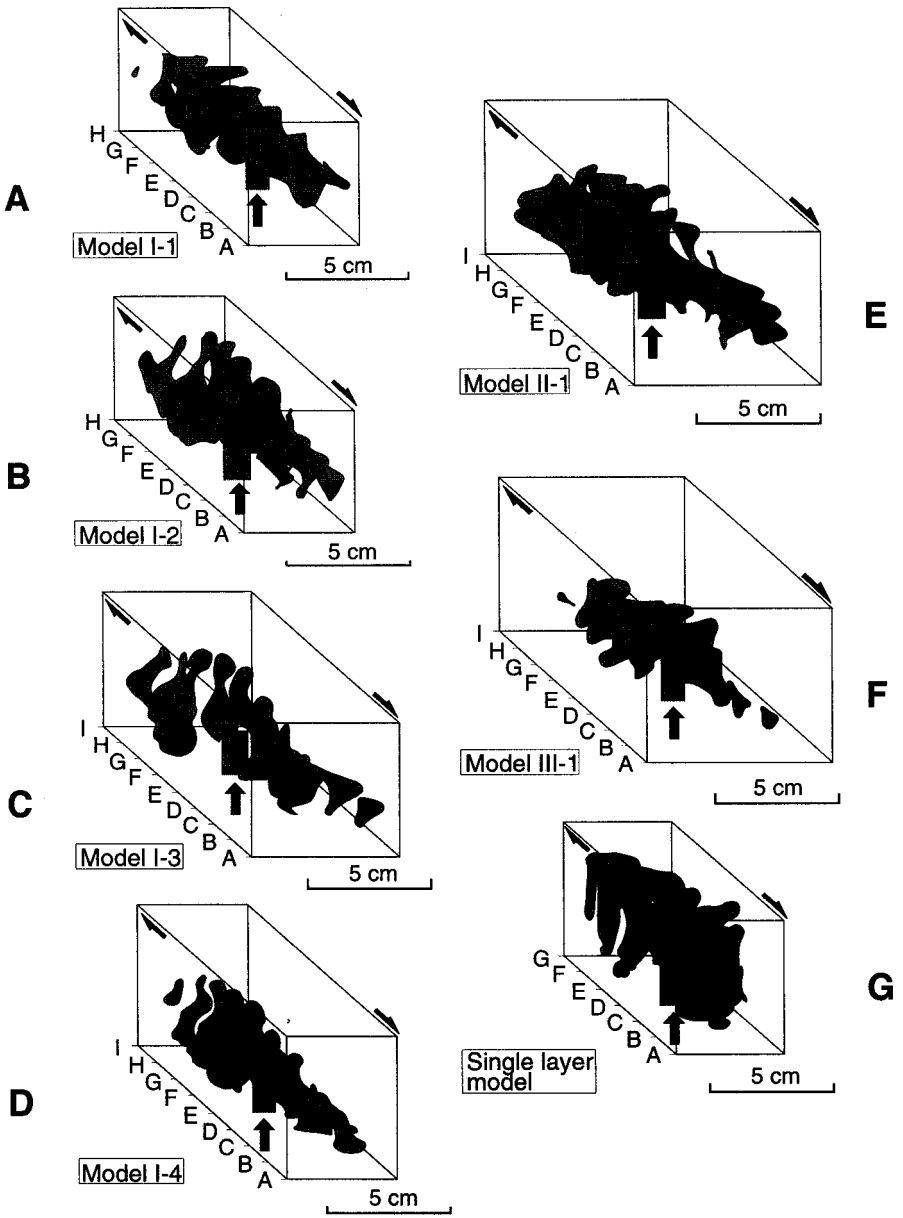

Fig. 5. 3D diagrams showing intrusion shapes in representative models; (A) model I-1, (B) model I-2, (C) model I-3, (D) model I-4, (E) model II-1, (F) model III-1, (G) single layer model. Letters A to I refer to serial sections (fig. 2C) made across models and used for drawing figures 6 and 8.

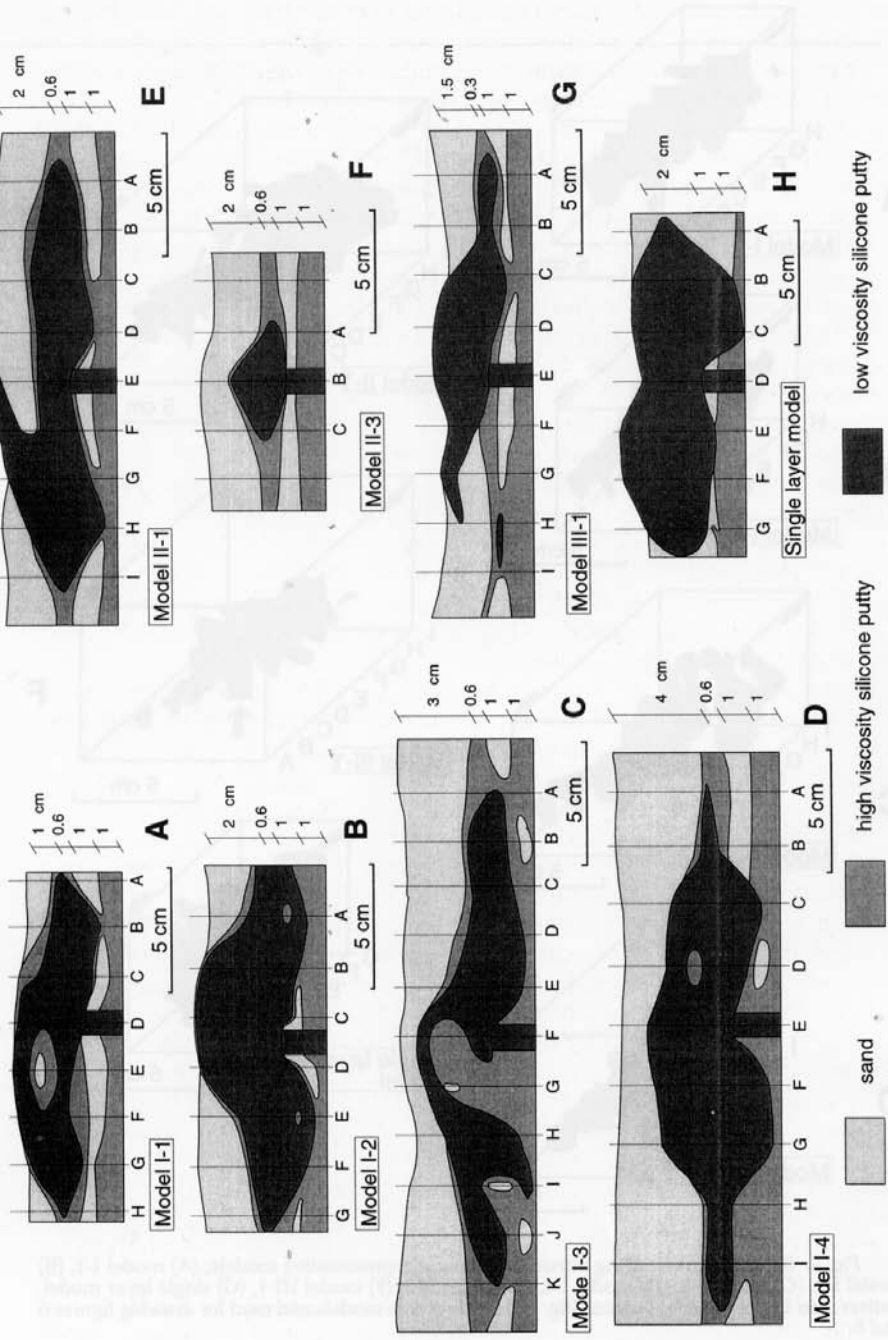

Fig. 6. Vertical cross sections parallel to the direction of maximum elongation of representative intrusions; (A) model I-1, (B) model I-2, (C) model I-3, (D) model I-4, (E) model II-1, (F) model II-3, (G) model III-1, (H) single layer model. Letters (A) to (K) refer to serial cross sections (fig. 5) used to make the drawing.

overburden (figs. 5G and 6H). Similar features were obtained by Román-Berdiel, Gapais, and Brun (1995) for injection in static environments. In contrast, three layer models allowed for intrusions of laccolithic type, with variable amounts of horizontal spreading along the weak layer (figs. 5A-F, 6A-F, and 7).

However, most intrusions are unconformable, some partially intruding the weak layer (models I-3 and I-4, fig. 6C and D) and (or) injecting along faults in the overburden (fig. 7), while others pierced the entire overburden thickness (models I-1, I-2 and III-1, fig. 6A, B, and G). From this, we note that most experimental conditions chosen correspond to intermediate situations between the field of piercing intrusions and the field of conformable laccoliths as defined by Román-Berdiel, Gapais, and Brun (1995) (fig. 3).

Interactions between faults and intrusion.–The combination of horizontal spreading and of piercing of the overburden yielded intrusion shapes that are commonly very irregular (fig. 5). Local interactions between faults and intrusion further induced irregular intrusion shapes. Thus, the attitude of intrusion walls can vary from strongly convex as a result of substantial horizontal spreading along the weak layer (figs. 5E and 7) to subvertical (fig. 5D) where spreading of the injected material was stopped by an active strike-slip fault (fig. 7).

In addition, the strike-slip environment favored local diking of injected material along faults throughout the sand overburden (fig. 7 and model II-1, fig. 6E). Similar features, which yield irregular shapes of intrusion roof, were also observed above laccoliths formed in an extensional regime (Román-Berdiel, Gapais, and Brun, 1995).

Intrusion in the middle of the strike-slip zone.–Reconstructed horizontal maps at depth show that intrusions emplaced in the middle of the strike-slip zone are always elongate in the extension field defined by the strike-slip deformation (fig. 8). Comparison of models II-1 and I-2 with model II-3 (compare fig. 8A and C with 8F), where the amounts of total strike-slip displacement are 19.8, 20, and 9.6 cm, respectively (table 2), emphasizes that the angle between the long axis of intrusions decreases consistently with increasing shear strain. Horizontal cross sections (fig. 8) further show that the amount of bulk shear strain γ can be roughly estimated using an overall shear zone width of 3 cm, which actually corresponds to the spacing between the two mobile basal plates. Making this calculation yields theoretical angles θ between the principal stretch direction and the shear zone boundary ($\tan 2\theta = 2/\gamma$) of 8°.4 and 15°.5 for models II-1 and I-2 (fig. 8A and C, $\gamma = 6.6$ and 6.7) and model II-3 (fig. 8F, $\gamma = 3.2$), respectively. These values are quite close to the observed angles θ' between the long axes of intrusions and the shearing direction (models II-1, I-2, and II-3, fig. 8A, C, and F, and table 3), and do not seem influenced by the size of the intrusion (compare models II-1, I-2 and II-3, fig. 8A, C, and F). This feature is observed even where intrusions are substantially deformed by faults (fig. 8D and E). From this, we infer that the long axis of model intrusions tends to track the long axis of the bulk strain ellipsoid. However, experiments suggest that the thickness of the overburden can influence the average orientation of the pluton (compare models I-1 to I-4, fig. 8B-E). Quantitative estimates of the amount of shear strain from pluton orientations are therefore probably of limited quality.

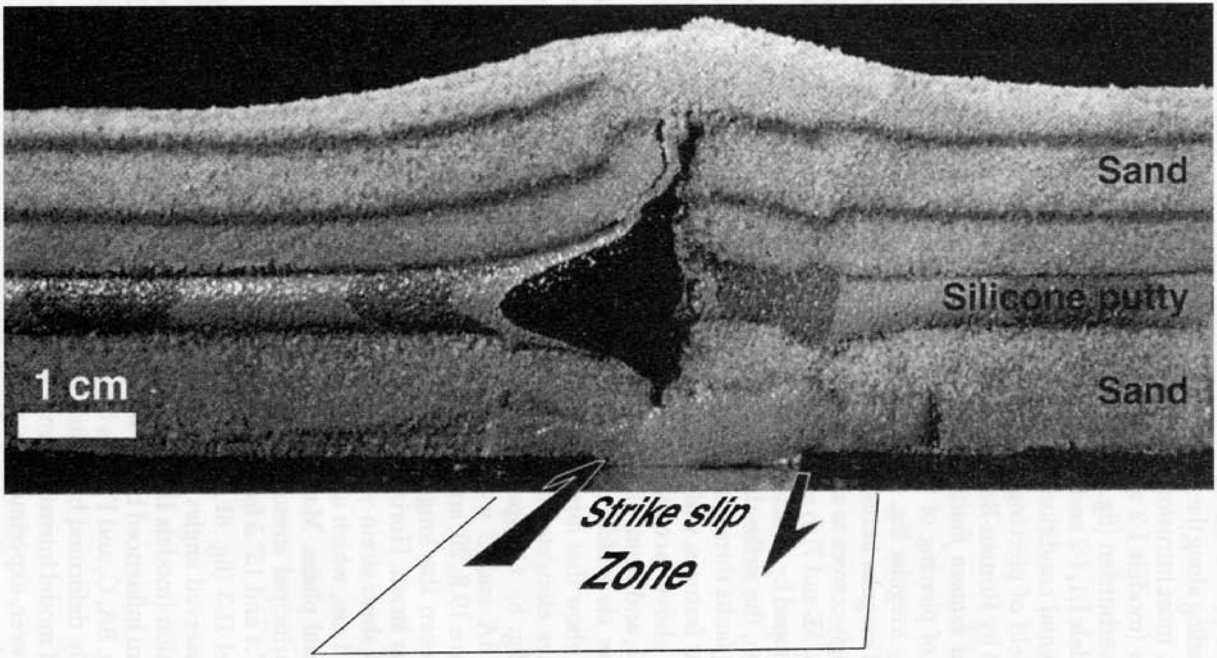

Fig. 7. Photograph showing section of model II-1 (see table 2 for model characteristics) cut across intrusion and perpendicular to strike-slip zone. Photograph shows typical features of model intrusions: space for intrusion is mainly created by preferential lateral expansion within the weak silicone layer (left-hand side of intrusion), and by lifting of overburden, lateral expansion is locally limited by faults and local diking of intrusion occurs along faults (right-hand side vertical intrusion boundary).

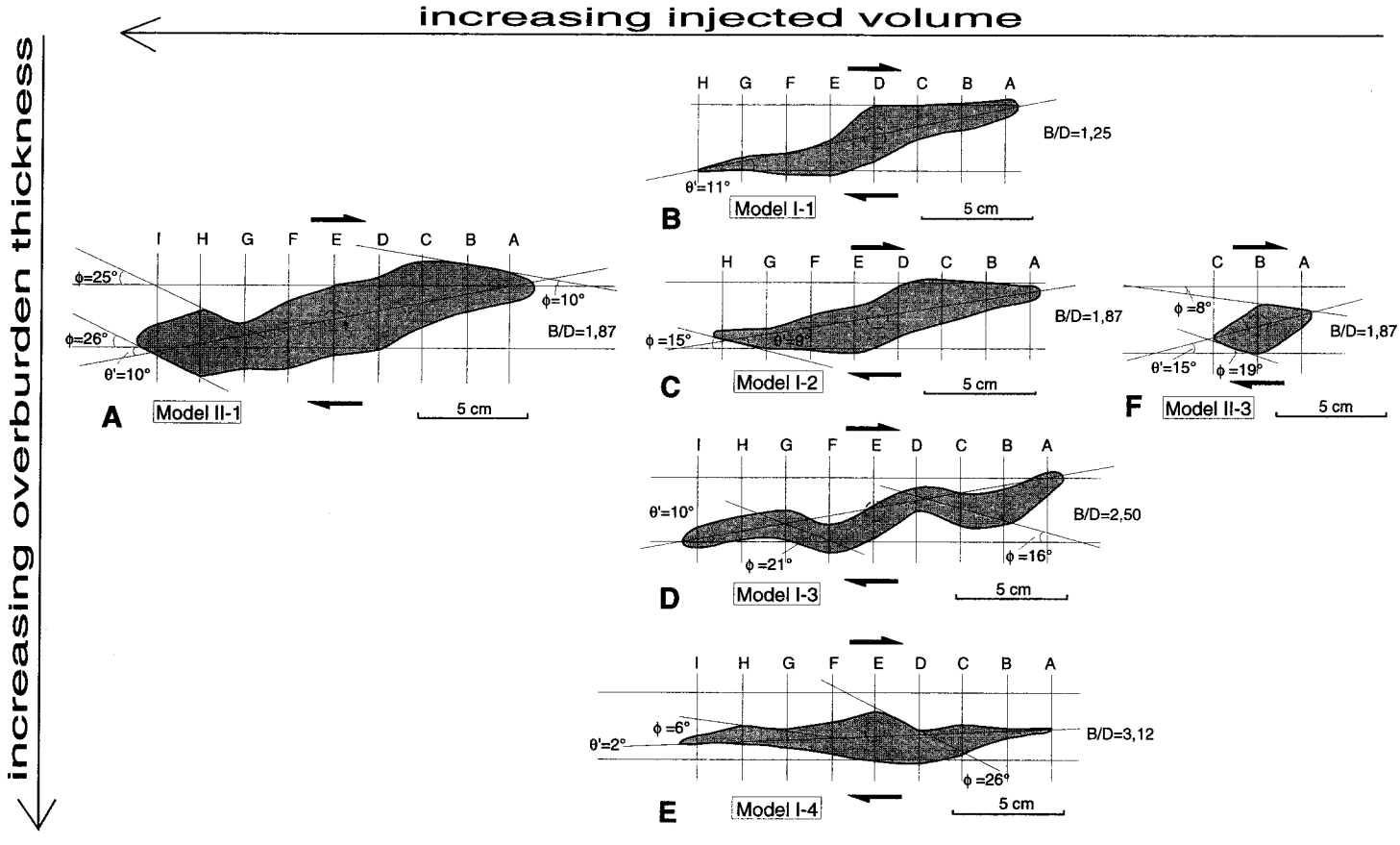

Fig. 8. Horizontal sections across representative intrusions; (A) model II-1, (B) model I-1, (C) model I-2, (D) model I-3, (E) model I-4, (F) II-3. Letters A to I refer to serial cross sections (fig. 5) used to make the drawing. B/D ratio is the thickness ratio between sand overburden and weak interbedded silicone layer. θ', angle between long axis of intrusion and bulk shearing direction. Φ, local angle between intrusion boundary and bulk shearing direction (see table 3). The two horizontal lines are 3 cm apart and correspond to the traces of the 2 basal velocity discontinuities. Dotted circle is the trace of the underlying feeding pipe.

Faults control the local shape of intrusion boundaries (figs. 4, 7, and 8). Thus, the orientations of many segments of intrusion boundaries seen on reconstructed maps (angle ϕ, table 3 and fig. 8) are subparallel to synthetic faults observed on the surface of the models (angle α, table 3 and fig. 4). For a weak layer of constant thickness, the influence of oblique synthetic faults on intrusion shapes is particularly strong given a relatively thick overburden (models I-3, I-4, fig. 8D and E); whereas with decreasing overburden thickness, the lateral expansion tends to be limited by faults subparallel to the boundary of the shear zone (models I-1, I-2, fig. 8B and C).

At depth, the control of the fault pattern on the local geometry of the intrusion leads to sigmoidal or lozenge intrusion shapes, especially for moderate thickness ratios between sand overburden and weak silicone layer (fig. 8). Intrusions limited by two major faults show typical lozenge shapes (models I-1, I-2, and II-3, fig. 8B, C, and F). However, in the vertical plane, intrusions have more irregular geometries due to local diking of injected material along faults throughout the sand overburden (fig. 7 and model II-1, fig. 6E).

Intrusions beside shear zones.–Models where the feeding pipe was located in the fixed basal plate beside a single velocity discontinuity induced asymmetric intrusion shapes (models IV-1 and IV-2, fig. 9).

In this type of experiments, injection within a homogeneous three-layer model resulted in a flat intrusion with shapes of asymmetric drop marked by a sheared tail trailing behind the intrusion (model IV-1, fig. 9A).

Another experiment, where the weak layer was present above the mobile plate and absent on the other side of the shear zone, above the feeding pipe, resulted in less asymmetric intrusion (model IV-2, fig. 9B). In this model, a well-developed sheared tail formed where the weak layer was present; whereas the lateral expansion of the pluton was limited above the feeding pipe.

These models emphasize the role of both weak layer and faults on pluton expansion. Thus, when the weak layer is absent above the feeding pipe, the intrusion expands preferentially toward the weak layer and cuts across the main shear zone (fig. 9B). In contrast, the expansion tends to be limited by the main shear zone when a weak layer is present on both sides of the zone, leading to a strongly asymmetric shape (fig. 9A). This asymmetry would be further marked in experiments made with a soft layer above the feeding pipe and absent on the other side of the shear zone.

COMPARISON WITH NATURE

Limits of model relevance.–In our experiments, space for intrusion is obtained by pushing aside the weak layer of country-rocks and lifting the overburden (fig. 7). Our models are thus consistent with inferences of Paterson and Fowler (1993a) who argued that one way of making space for magmas in the crust is to displace the earth surface upward.

Diking also occurs locally along faults in our models (fig. 7). Horizontal cross sections (fig. 8) further suggest that diking occurred preferentially along Riedel faults. This could reflect preferential diking along zones of maximum

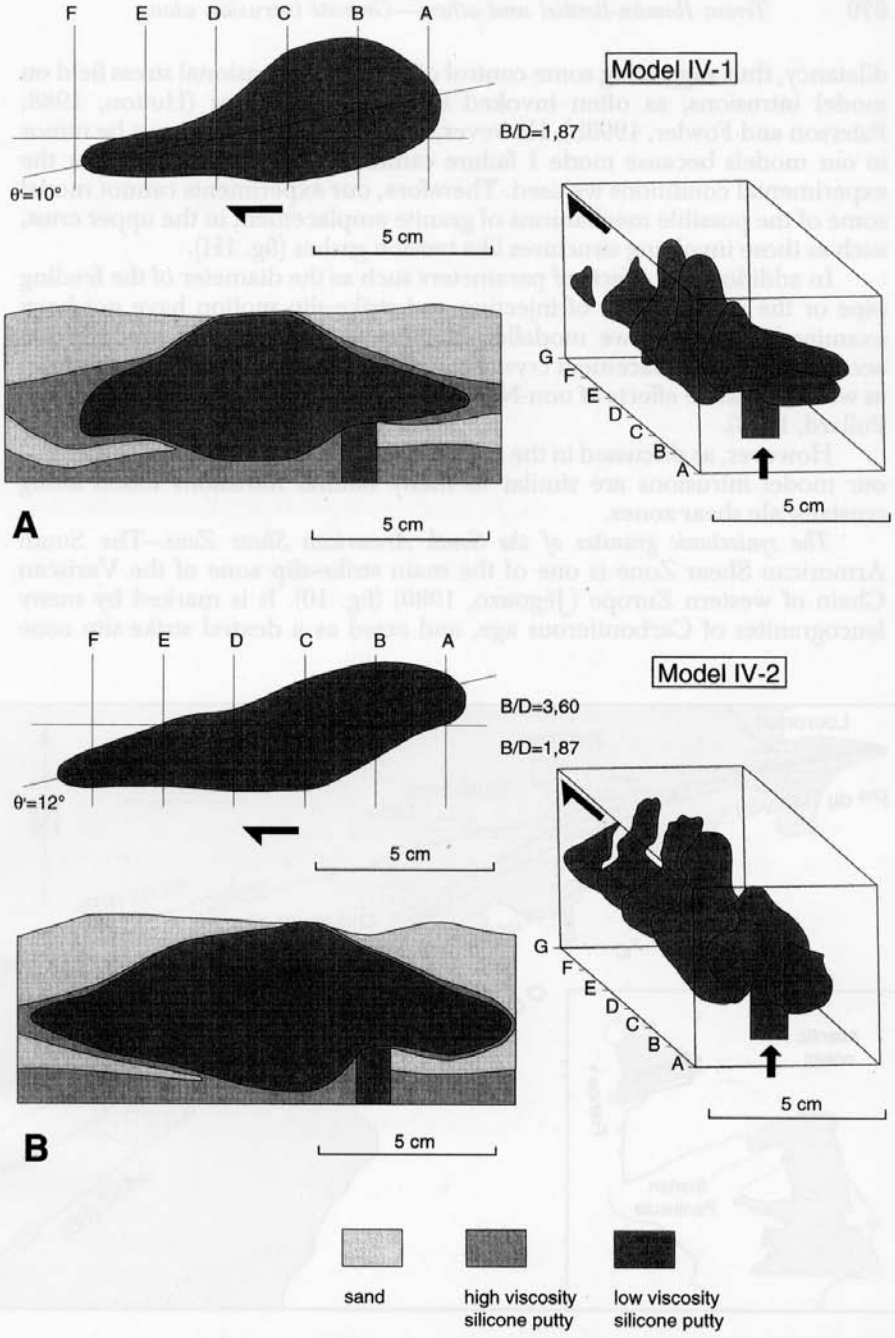

Fig. 9. 3D diagrams, horizontal sections, and vertical sections for strike-slip experiments made with a feeding pipe (dotted circle on maps) located beside a single basal velocity discontinuity. Letters A to G refer to serial cross sections (fig. 2C) used to make the drawing. Vertical cross sections are parallel to the direction of intrusion elongation. B/D is the thickness ratio between sand overburden and interbedded silicone layer. θ′ is angle between long axis of intrusion and bulk shearing direction (see table 3).

dilatancy, thus suggesting some control of the local extensional stress field on model intrusions, as often invoked in natural situations (Hutton, 1988; Paterson and Fowler, 1993b). However, such possible control must be minor in our models because mode 1 failure cannot be produced in sand for the experimental conditions we used. Therefore, our experiments cannot model some of the possible mechanisms of granite emplacement in the upper crust, such as those involving structures like tension gashes (fig. 1H).

In addition, the effects of parameters such as the diameter of the feeding pipe or the relative rates of injection and strike-slip motion have not been examined. Nor have we modelled changes of viscosity and strength that accompany synemplacement crystallisation and cooling of natural intrusions, as well as possible effects of non-Newtonian magma rheologies (Johnson and Pollard, 1973).

However, as discussed in the examples below, the geometries of many of our model intrusions are similar to many natural intrusions found along crustal-scale shear zones.

The syntectonic granites of the South Armorican Shear Zone.–The South Armorican Shear Zone is one of the main strike-slip zone of the Variscan Chain of western Europe (Jégouzo, 1980) (fig. 10). It is marked by many leucogranites of Carboniferous age, and acted as a dextral strike-slip zone

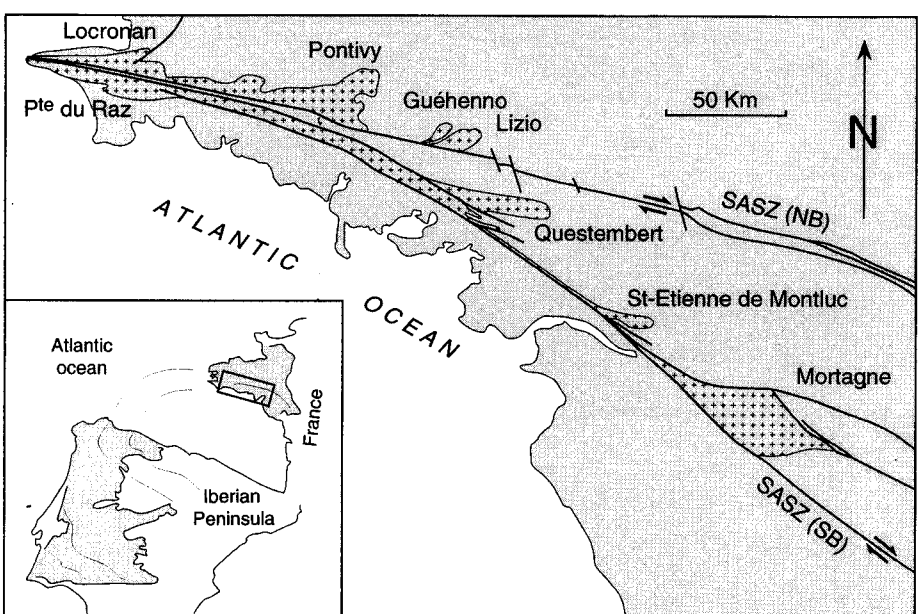

Fig. 10. Sketch map of the southern part of the Armorican Massif (western France) and its location in the Variscan belt of western Europe. SASZ, South Armorican Shear Zone; (NB), northern branch; (SB), southern branch. Syntectonic leucogranites associated with the shear zone are shown with crosses.

during Carboniferous times (Jégouzo, 1980). Geometrical characteristics of syntectonic plutons were first established in this zone (Berthé, Choukroune, and Jégouzo, 1979; Berthé, Choukroune, and Gapais, 1979; Jégouzo, 1980), including S-C fabrics.

As most Carboniferous plutons of the Variscan Chain, the Armorican leucogranites have generally emplaced at relatively shallow levels (Vigneresse and Brun, 1983). Many of them intrude pelitic sediments of low to medium metamorphic grade, which constitute the lower part of an upper Proterozoic to Paleozoic sedimentary cover lying on a Precambrian basement. Gravimetric data have shown that these granites have a generally flat, horizontally elongate form with a gently dipping or subhorizontal floor (Vigneresse and Brun, 1983). For many of them, 95 percent of their present volume is located at depths less than 5 km (Vigneresse and Brun, 1983).

Diapirism has been frequently invoked for the ascent and the emplacement of the Armorican leucogranites (Hanmer and Vigneresse, 1980; Vigneresse and Brun, 1983). However, recent works have emphasized that diapirism is generally not a convenient mechanism to explain plutons emplaced at shallow crustal levels because such locations imply that the magma has risen through a substantial thickness of brittle upper crust before it emplaced (see Brun and others, 1990; Clemens and Mawer, 1992). In fact, most Armorican plutons are laccoliths emplaced by "in situ" lateral expansion in a relatively weak sedimentary cover after rising of the magma along fractures throughout an underlying resistant basement (Brun and others, 1990; Lagarde, Brun, and Gapais, 1990).

Several Armorican leucogranites are strongly mylonitized and are extensively stretched along the South Armorican Shear Zone (fig. 10). The less deformed plutons show two main types of geometries according to their relationships with major fault zones (fig. 10): asymmetric drop-shaped plutons, located along a single fault zone (for example, Pontivy, Lizio, or Questembert granites) and lozenge-shaped plutons located between two fault zones (for example, Mortagne granite). These two types of intrusions are discussed in detail below.

Asymmetric drop-shaped plutons.–Asymmetric drop-shaped plutons are numerous along the South Armorican Shear Zone (fig. 10). This geometry occurs because a strong shear strain gradient at the vicinity of the main fault zone led to the development of a sheared tail trailing behind the intrusion (fig. 1B). It is typical of many granites associated with major strike-slip zones. Examples include the Ardara pluton in Ireland (Holder, 1978; Hutton, 1988), the Brovales granite in southern Spain (Brun and Pons, 1981), the Ash Sha'b granite in northern Saudi Arabia (Davies, 1982), or some massifs from the Saraya Batholith in eastern Senegal (Pons, Oudin, and Valero, 1992).

Several detailed structural studies have been made on the Lizio granite (figs. 10 and 11) (Berthé, Choukroune, and Jégouzo, 1979; Berthé, Choukroune, and Gapais, 1979; Jégouzo, 1980; Vigneresse and Brun, 1983). Its floor dips gently down to about 8 km depth in the northeastern part of the massif (fig. 11) (Vigneresse and Brun, 1983). This zone is significantly shifted with respect to the main fault zone and could correspond to the feeding zone

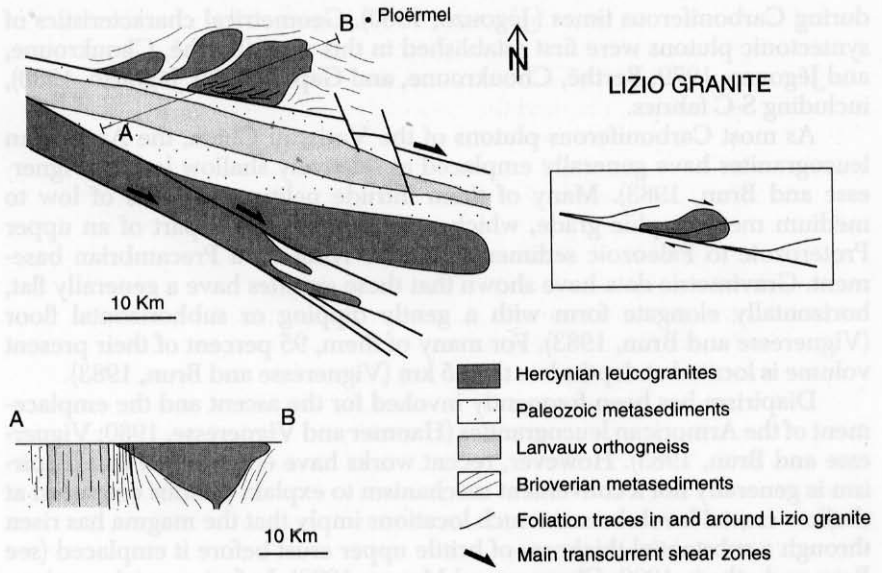

Fig. 11. Geological and structural sketch map and cross section of the area around the Lizio granite (located on fig. 10) (modified after Jégouzo, 1980, and Jégouzo and Rossello, 1988). Cross section (A-B) parallel to the long axis of pluton is drawn from gravimetric data (Vigneresse and Brun, 1983). Horizontal and vertical scales are similar. Inset shows general sketch of model kinematic context which can compare to the natural example.

of the massif (Vigneresse and Brun, 1983). To the south, the sheared tail of the pluton is mainly made of S-C mylonites (Berthé, Choukroune, and Jégouzo, 1979).

This natural example is quite similar to our model IV-1 (fig. 9A), whose feed pipe is shifted with respect to the strike-slip zone. On the map, the massif is elongate in a northeast-southwest direction consistent with dextral strike-slip motion along the main fault zone (fig. 11). The cross section parallel to pluton elongation further suggests northeast-southwest lateral expansion (fig. 11). The map and cross sections of the Lizio area also show that most of the granite is located on the northern side of the main fault zone (fig. 11).

Our models have shown the strong influence of the occurrence of a weak crustal layer on the degree of lateral expansion of intrusions. The Lizio granite was emplaced within weak Brioverian (Upper Proterozoic to Cambrian in age) pelitic metasediments located North of the main fault zone (fig. 11). These sediments are the lowermost soft unit above the Precambrian basement and are overlain by a thick (up to 600 m) quartzite unit of early Ordovician age. They are thus comparable to the weak layer in our models. In contrast, south of the main fault zone, lithologies are more competent, mainly made of orthogneisses (Lanvaux orthogneiss) and of volcanoclastic deposits of Lower Paleozoic age (fig. 11). These differences in lithologies on

both sides of the main fault zone have probably limited the southward lateral expansion of the pluton.

Lozenge-shaped plutons.–Lozenge-shaped plutons are commonly associated with strike-slip zones, and the creation of voids, such as pull-aparts (fig. 1F, 1G), has often been invoked for their emplacement (see review by Hutton, 1988).

The Mortagne granite (fig. 10) is a particularly remarkable example. Indeed, its lozenge shape and its location between two strike-slip zones (fig. 12) led Guineberteau, Bouchez, and Vigneresse (1987) to propose that this massif emplaced in a pull-apart. This example is now commonly cited as a classical example of this type of emplacement (see Pitcher, 1992).

According to the general geometry of the Mortagne granite (fig. 12), an emplacement in a pull-apart would imply sinistral strike-slip parallel to the South Armorican Shear Zone (Guineberteau, Bouchez, and Vigneresse, 1987). However, all other authors who worked in the area have argued that the motion along the South Armorican Shear Zone during the emplacement of all Carboniferous granites was dextral (see reviews by Jégouzo, 1980, and Gapais and Le Corre, 1980). Beside regional arguments (Gapais and Le Corre, 1980), a hypothesis of syn-emplacement sinistral shearing does not hold for the following reasons.

The Mortagne granite has been dated at 315 ± 15 Ma (Rb/Sr whole rock, Bernard-Griffith and others, 1985). All other dated leucogranites of the South Armorican Shear Zone have comparable ages (see review by Le Corre and others, 1991). In particular, the Questembert granite and the Pointe du Raz granite, which are located on the same shear zone as the Mortagne granite (fig. 10), have been dated at 329 ± 20 Ma and 301 ± 18 Ma, respectively (Rb/Sr whole rock, Bernard-Griffith and others, 1985). These two granites are almost entirely composed of S-C mylonites which show dextral shearing only (Jégouzo, 1980).

As pointed out by Guineberteau, Bouchez, and Vigneresse (1987), the latest movements along the major faults that bound the massif to the northeast and to the southwest are clearly dextral and occurred during cooling of the massif down to greenschist facies metamorphic conditions. Cooling rates for upper-crustal plutons are generally high, especially during the first stages of cooling (Spera, 1980; Paterson and Tobisch, 1992), and average internal temperatures comparable to that of country-rocks are typically reached within ~1 Ma (Spera, 1980). If sinistral strike-slip motion occurred parallel to the South Armorican Shear Zone, this would have been a rather short-lived anomaly in an overall tectonic context of dextral strike-slip.

Guineberteau, Bouchez, and Vigneresse (1987) provided a detailed map of the internal structures of the Mortagne granite. Traces of foliation planes are shown in figure 12. They indicate bulk north-northeast-south-southwest shortening of the massif, irrespective of their associated thermal conditions. Most mineral lineations strike consistently northwest-southeast and are generally gently plunging. The overall internal pattern is locally disturbed by conjugate sinistral shear zones which also indicate north-northeast-south-southwest shortening. The occurrence of sinistral strike-slip along the south-

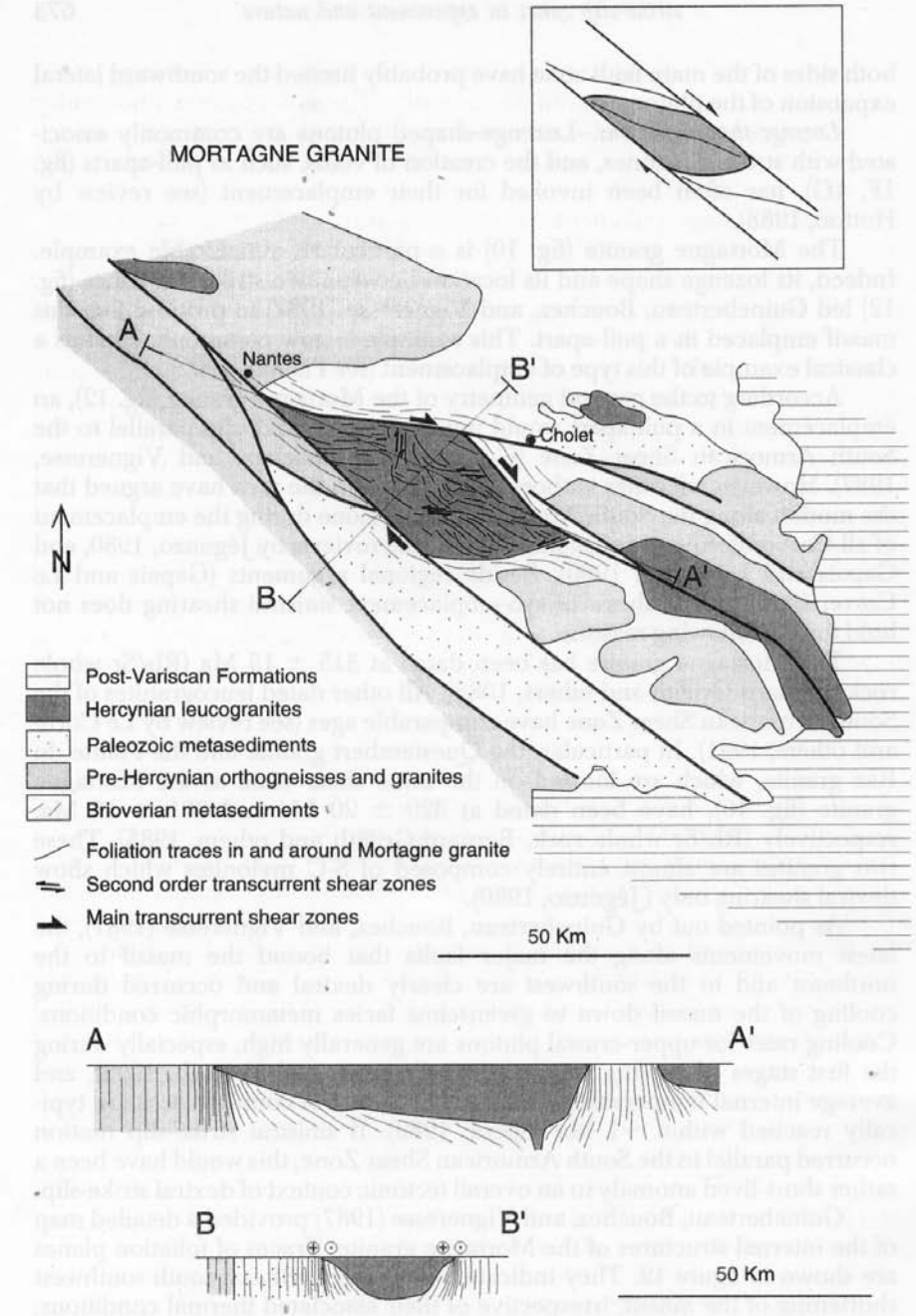

Fig. 12. Geological and structural sketch map and cross sections of the area around the Mortagne pluton (located on fig. 10) (modified after Guineberteau, Bouchez, and Vigneresse, 1987; Le Corre and others, 1991). Cross sections A-A′ and B-B′ are drawn from gravimetric data (Guineberteau, Bouchez, and Vigneresse, 1987). Structural data are from Guineberteau, Bouchez, and Vigneresse (1987). Horizontal and vertical scales are similar. Inset shows general sketch of model kinematic context which can compare to the natural example.

ern boundary of the pluton (Guineberteau, Bouchez, and Vigneresse, 1987) (fig. 12) is also compatible with north-northeast-south-southwest shortening. An overall north-northeast-south-southwest shortening direction is not compatible with northwest-southeast directed sinistral strike-slip but instead indicates dextral strike-slip.

Thus, geologic and geometric evidence shows that the Mortagne granite was emplaced during dextral strike-slip motion along the South Armorican Shear Zone.

A detailed gravimetric study (Guineberteau, Bouchez, and Vigneresse, 1987) has shown that the floor of the pluton is generally flat, except along the shear zones that define the northeast and southwest boundaries of the pluton, and at the southeastern termination of the massif where floor depths exceed 10 ± 2 km (fig. 12). This latter zone is interpreted as the feeding pipe (Guineberteau, Bouchez, and Vigneresse, 1987). In cross sections, the massif is strongly asymmetric (fig. 12), with a pronounced lateral expansion toward the northwest. This direction is compatible with preferential expansion of the pluton along a bulk stretch direction imposed by dextral regional strike-slip.

Our experiments showed that model intrusions which spread preferentially in the extension direction associated with the strike-slip motion yield overall patterns similar to those observed for the Mortagne pluton. This massif compares particularly well to lozenge-shaped model intrusions located between two major faults (fig. 8B, C and F).

CONCLUSIONS

1. Our model experiments of intrusion into a brittle crust deformed by strike-slip shearing show that the occurrence of an incompetent level between two competent units serves to localize laccolithic bodies. This conclusion is consistent with experimental results of Román-Berdiel, Gapais, and Brun (1995).

2. Intrusions into strike-slip zones are elongate as a result of preferential lateral expansion in the principal extension direction determined by the bulk strain field. This direction controls the emplacement beginning with the first stages of injection.

3. Faults formed in the overburden limit the lateral expansion of the intrusions, leading to local parallelism between faults and intrusion boundaries. For a constant thickness of the weak layer, this effect increases with increasing overburden thickness.

4. For moderate brittle/ductile thickness ratios of model country-rocks, the control of faults on the lateral expansion results in intrusions of sigmoidal or lozenge shapes, bounded by two parallel strike-slip faults. This effect decreases with increasing brittle/ductile ratio of model country-rocks.

5. The strike-slip environment allowed local rising of the injected fluid along faults formed in the overburden.

6. Feeding pipes shifted with respect to the middle of the strike-slip zone result in asymmetric intrusions, with the development of a sheared tail trailing behind the intrusion.

7. Our model intrusions illustrate that the room problem is not a critical factor to explain the shape of many plutons emplaced along strike-slip zones. In particular, intrusion between two faults can yield typical lozenge-shaped plutons for which emplacement mechanisms like those involving pull-aparts are irrelevant.

8. Models account for the two main types of map patterns of synkinematic plutons emplaced along the South Armorican Shear Zone: asymmetric plutons with a sheared tail and lozenge shape plutons.

ACKNOWLEDGMENTS

We thank J.J. Kermarrec (Géosciences Rennes) who made and maintained the experimental apparatus and helped with the experiments. P. Rajlich made useful suggestions on early drafts of the manuscript. Reviews by J. Dixon, B. Tikoff, and an anonymous reviewer were particularly useful to improve the manuscript. This work was supported by the Spanish Ministry of Education and Science (research grant to T.R.B.).

REFERENCES

Aranguren, A., and Tubía, J. M., 1992, Structural evidence for the relationship between thrusts, extensional faults and granite intrusions in the Variscan belt of Galicia (Spain): Journal of Structural Geology, v. 14, p. 1229–1237.

Ballard, J. F., Brun, J. P., Van den Driessche, J., and Allemand, P., 1987, Propagation des chevauchements au-dessus des zones de décollement: modèles experimentaux: Comptes Rendus de l'Académie des Sciences de Paris, v. 305, p. 1249–1253.

Basile, C., 1990, Analyse structurale et modélisation analogique d'une marge transformante. Exemple de la marge de Côte d'Ivoire-Ghana: Mémoires et Documents du Centre Armoricain d'Etude Structurale des Socles, v. 39, 220 p.

Bernard-Griffiths, J., Peucat, J. J., Sheppard, S., and Vidal, P., 1985, Petrogenesis of Hercynian leucogranites from South Armorican massif. Contribution of REE and isotopic (Sr, Nd, Pb, O) geochemical data to the study of source rock characteristics and ages: Earth and Planetary Science Letters, v. 74, p. 235–250.

Berner, M., Ramberg, H., and Stephansson, O., 1972, Diapirism in theory and experiment: Tectonophysics, v. 15, p. 197–218.

Berthé, D., Choukroune, P., and Gapais, D., 1979, Orientations préférentielles du quartz et orthogneissification progressive en régime cisaillant: l'exemple du cisaillement sud-armoricain: Bulletin de Minéralogie et Cristallographie, v. 102, p. 265–272.

Berthé, D., Choukroune, P., and Jégouzo, P., 1979, Orthogneiss, mylonite and non coaxial deformation of granites: the example of the South Armorican Shear Zone: Journal of Structural Geology, v. 1, p. 31–42.

Brun, J. P., Gapais, D., Cogné, J. P., Ledru, P., and Vigneresse, J. L., 1990, The Flamanville granite (Northwest France): an unequivocal example of a syntectonically expanding pluton: Geological Journal, v. 25, p. 271–286.

Brun, J. P., and Pons, J., 1981, Strain patterns of pluton emplacement in a crust undergoing non-coaxial deformation, Sierra Morena, Southern Spain: Journal of Structural Geology, v. 3, p. 219–229.

Castro, A., 1986, Structural pattern and ascent model in the Central Extremadura batholith, Hercynian belt, Spain: Journal of Structural Geology, v. 8, p. 633–645.

—— 1987, On granitoid emplacement and related structures. A review: Geologische Rundschau, v. 76, p. 101–124.

Clemens, J. D., and Mawer, C. K., 1992, Granitic magma transport by fracture propagation: Tectonophysics, v. 204, p. 339–360.

Cloos, H., 1928, Experimente zur inneren Tektonic: Zentralblatt für Mineralogie Geologie und Paläontologie, v. 1928 B, p. 609–621.

Cruden, A., 1990, Flow and fabric development during the diapiric rise of magma: Journal of Geology, v. 98, p. 681–698.

Davies, F. B., 1982, Pan-African granite intrusion in response to tectonic volume changes in a ductile shear zone from Northern Saudi Arabia: Journal of Geology, v. 90, p. 467–483.

Dixon, J. M., 1975, Finite strain and progressive deformation in models of diapiric structures: Tectonophysics, v. 28, p. 89–124.

Dixon, J. M., and Simpson, D. G., 1987, Centrifuge modelling of laccolith intrusion: Journal of Structural Geology, v. 9, p. 87–103.
D'Lemos, R. S., Brown, M., and Strachan, R. A., 1992, Granite magma generation; ascent and emplacement within a transpressional orogen: Journal of the Geological Society of London, v. 149, p. 487–490.
Emmons, R. C., 1979, Strike-slip rupture pattern in sand models: Tectonophysics, v. 7, p. 71–87.
Gapais, D., Fiquet, G., and Cobbold, P. R., 1991, Slip system domains, 3. New insights in fault kinematics from plane-strain sandbox experiments: Tectonophysics, v. 188, p. 143–157.
Gapais, D., and Le Corre, C., 1980, Is the Hercynian belt of Brittany a major shear zone?: Nature, v. 288, p. 574–575.
Grout, F. F., 1945, Scale models of structures related to batholiths: American Journal of Science, v. 243, p. 260–284.
Guineberteau, B., Bouchez, J. L., and Vigneresse, J. L., 1987, The Mortagne granite pluton (France) emplaced by pull-apart along a shear zone: structural and gravimetric arguments and regional implication: Geological Society of America Bulletin, v. 99, p. 763–770.
Hanmer, S., and Vigneresse, J. L., 1980, Mise en place de diapirs syntectoniques dans la chaîne hercynienne: exemple des massifs leucogranitiques de Locronan et de Pontivy (Bretagne centrale): Bulletin de la Société Géologique de France, v. 7, p. 193–202.
Holder, M. T., 1978, Granite emplacement models: Journal of the Geological Society of London, v. 135, p. 459–464.
Hoppener, R., Kalthoff, E., and Schrader, P., 1969, Zur Physicalischen Tektonik: Bruchbildung bei verschiedenen affinen Deformationen im Experiment: Geologische Rundschau, v. 59, p. 179–193.
Howe, E., 1901, Experiments illustrating intrusion and erosion: Washington, D.C., United States Geological Survey 21st Annual Report, p. 291–303.
Hubbert, M. K., 1937, Theory of scale models as applied to the study of geologic structures: Geological Society of America Bulletin, v. 48, p. 1459.
Hurlbut, C. S., and Griggs, D. T., 1939, Igneous rocks of the Highwood Mountains, Montana-I. The laccoliths: Geological Society of America Bulletin, v. 50, p. 1043–1112.
Hutton, D. H. W., 1981, The structural setting of the Main Donegal Granite; a reply to comments on a recent interpretation: Geological Journal, v. 16, p. 149–151.
—— 1982, A tectonic model for the emplacement of the Main Donegal Granite, NW Ireland: Journal of the Geological Society of London, v. 139, p. 615–631.
—— 1988, Granite emplacement mechanisms and tectonic controls: inferences from deformation studies: Transactions of the Royal Society of Edinburg: Earth Sciences, v. 79, p. 245–255.
Hutton, D. H. W., Dempster, T. J., Brown, P. E., and Becker, S. D., 1990, A new mechanism of granite emplacement: intrusion in active extensional shear zones: Nature, v. 343, p. 452–455.
Iglesias, M., and Choukroune, P., 1980, Shear zones in the Iberian Arc: Journal of Structural Geology, v. 2, p. 63–68.
Jégouzo, P., 1980, The South Armorican shear zone: Journal of Structural Geology, v. 2, p. 39–47.
Jégouzo, P., and Rossello, E. A., 1988, La Branche Nord du Cisaillement Sud-Armoricain (France): un essai d'évaluation du déplacement par l'analyse des mylonites: Comptes Rendus de l'Académie des Sciences de Paris, v. 307, p. 1825–1831.
Johnson, A. M., and Pollard, D. D., 1973, Mechanics of growth of some laccolithic intrusions in the Henry Mountains, Utah, I. Field observations, Gilbert's model, physical properties and flow of the magma: Tectonophysics, v. 18, p. 261–309.
Krantz, R. W., 1991, Measurements of friction coefficients and cohesion for faulting and fault reactivation in laboratory models using sand and sand mixtures: Tectonophysics, v. 188, p. 203–207.
Lagarde, J. L., Ait-Omar, S., and Roddaz, B., 1990, Structural characteristics of granitic plutons emplaced during weak regional deformation: examples from late Carboniferous plutons, Morocco: Journal of Structural Geology, v. 12, p. 805–821.
Lagarde, J. L., Brun, J. P., and Gapais, D., 1990, Formation des plutons granitiques par injection et expansion latérale dans leur site de mise en place: une alternative au diapirisme en domaine épizonal: Comptes Rendus de l'Académie des Sciences de Paris, v. 310, p. 1109–1114.
Le Corre, C., Auvray, B., Ballèvre, M., and Robardet, M., 1991, Le Massif Armoricain: Sciences Géologiques, Bulletin, v. 44, p. 31–103.
McCaffrey, K. J. W., 1992, Igneous emplacement in a transpressive shear zone: Ox Mountains igneous complex: Journal of the Geological Society of London, v. 149, p. 221–235.
McCarthy, G. R., 1925, Some facts and theories concerning laccoliths: Journal of Geology, v. 33, p. 1–18.
Mandl, G., De-Jong, L. N. J., and Maltha, A., 1977, Shear zones in granular material: Rock Mechanics, v. 9, p. 95–144.

Merle, O., and Vendeville, B., 1992, Modélisation analogique de chevauchements induits par des intrusions magmatiques: Comptes Rendus de l'Académie des Sciences de Paris, v. 315, p. 1541–1547.
Naylor, M. A., Mandl, G., and Sijpesteijn, C. H. K., 1986, Fault geometries in basement-induced wrench faulting under different initial stress states: Journal of Structural Geology, v. 8, p. 737–752.
Oertel, G., 1965, The mechanism of faulting in clay experiments: Tectonophysics, v. 2, p. 343–393.
Paterson, S. R., and Fowler, T. K., 1993a, Re-examining pluton emplacement processes: Journal of Structural Geology, v. 15, p. 191–206.
—— 1993b, Extensional pluton-emplacement models: Do they work for large plutonic complexes?: Geology, v. 21, p. 781–784.
Paterson, S. R., and Tobisch, O. T., 1992, Rates of processes in magmatic arcs: implications for the timing and nature of pluton emplacement and wall rock deformation: Journal of Structural Geology, v. 14, p. 291–300.
Pitcher, W. S., 1992, The nature and origin of granite: London, Blackie Academic Press, 321 p.
Pitcher, W. S., and Berger, A. R., 1972, The Geology of Donegal: a Study of Granite Emplacement and Unroofing: New York, Wiley Intersciences, 435 p.
Pitcher, W. S., and Bussell, M. A., 1977, Structural control of batholithic emplacement in Peru: a review: Journal of the Geological Society of London, v. 133, p. 249–256.
Pollard, D. D., and Johnson, A. M., 1973, Mechanics of growth of some laccolithic intrusions in the Henry Mountains, UTAH, II. Bending and failure of overburden layers and sill formation: Tectonophysics, v. 18, p. 311–354.
Pons, J., Oudin, C., and Valero, J., 1992, Kinematics of large syn-orogenic intrusions: example of the Lower Proterozoic Saraya batholith (Eastern Senegal): Geologische Rundschau, v. 81, p. 473–486.
Ramberg, H., 1970, Model studies in relation to intrusion of plutonic bodies. *in* Newall, G., and Rast, N., editors, Mechanisms of Igneous Intrusion: Liverpool, Gallery Press, p. 261–286.
—— 1981, Gravity, Deformation, and the Earth's Crust in Theory, Experiments and Geological Applications: London, Academic Press, 214 p.
Ramsay, J. G., 1989, Emplacement kinematics of a granite diapir: the Chindamora batholith, Zimbabwe: Journal of Structural Geology, v. 11, p. 191–209.
Richard, P., Ballard, J. F., Colletta, B., and Cobbold, P., 1989, Naissance et évolution de failles au-dessus d'un décrochement de socle: modélisation analogique et tomographie: Comptes Rendus de l'Académie des Sciences de Paris, v. 309, p. 2111–2118.
Richard, P., Loyo, B., and Cobbold, P., 1989, Formation simultanée de failles et de plis au-dessus d'un décrochement de socle: modélisation expérimentale: Comptes Rendus de l'Académie des Sciences de Paris, v. 309, p. 1061–1066.
Richard, P., Mocquet, B., and Cobbold, P. R., 1991, Experiments on simultaneous faulting and folding above a basement wrench fault: Tectonophysics, v. 188, p. 133–141.
Riedel, W., 1929, Zur mechanik geologischer Brucherscheinungen: Zentralblatt für Mineralogie Geologie und Paläontologie, v. 1929 B, p. 354–368.
Román-Berdiel, T., Gapais, D., and Brun, J. P., 1995, Analogue models of laccolith formation: Journal of Structural Geology, v. 17, p. 1337–1346.
Schmidt, C. J., Smedes, H. W., and O'Neill, J. M., 1990, Syncompressional emplacement of the Boulder and Tobacco Root Batholiths (Montana-USA) by pull-apart along old fault zones: Geological Journal, v. 25, p. 305–318.
Spera, F. J., 1980, Thermal evolution of plutons: A parameterized approach: Science, v. 207, p. 299–301.
Tchalenko, J. S., 1970, Similarities between shear zones of different magnitudes: Geological Society of America Bulletin, v. 81, p. 1625–1640.
Tikoff, B., and Teyssier, C., 1992, Crustal-scale, en échelon "P-shear" tensional bridges: a possible solution to the batholith room problem: Geology, v. 20, p. 927–930.
Vendeville, B., 1987, Champs de failles et tectonique en extension: Modélisation expérimentale: Mémoires et Documents du Centre Armoricain d'Etude Structurale des Socles, v. 15, 395 p.
Vendeville, B., Cobbold, P. R., Davy, P., Brun, J. P., and Choukroune, P., 1987, Physical models of extensional tectonics at various scales, *in* Coward, M. P., Dewey, J. F., and Hancock, P. L., editors, Continental Extensional Tectonics: Geological Society Special Publication, v. 28, p. 95–107.
Vigneresse, J. L., and Brun, J. P., 1983, Les leucogranites armoricains marqueurs de la déformation régionale: apport de la gravimétrie: Bulletin de la Société Géologique de France, v. 7, p. 357–366.
White, N., and Hutton, D. H. W., 1985, The structure of the Dalradian rocks in west Fanad, Conty Donegal: Irish Journal of Earth Science, v. 7, p. 79–92.
Wilcox, R. E., Harding, T. P., and Seely, D. R., 1973, Basic wrench tectonics: American Association of Petroleum Geologists Bulletin, v. 57, p. 74–96.